Comparison of direct flux measurements and emission factor based estimates of urban emissions

Julia Asplund
Master's thesis, 45 ECTS
Environmental Science, 2021

Comparison of direct flux measurements and emission factor based estimates of urban emissions

Author: Julia Asplund

Main supervisor: David Hadden, PhD
Secondary supervisor: Douglas Nilsson, Associate Professor

Abstract

As climate and air quality models improve, and informed policy strategies for mitigation become more urgent, the need for valid estimates of emissions on a local level is increasing, particularly in urban areas. Many cities have established emission inventories using a bottom-up approach. Emission estimates based on inventories can be compared to direct atmospheric flux measurements to validate emission models, and highlight sources or sinks that have not been accounted for. Such comparisons have been made at several sites in the US and Europe, with a large variation in results. This work features a first comparison between direct eddy covariance flux measurements and estimated emissions in Stockholm, using flux data from 2008-2009 and the emission database of the local department for environmental air- and noise pollution. The measurements included both CO_2 fluxes and aerosol fluxes in the size range 0.25-2.5μm. Averaged estimates of CO_2 emissions agreed with averaged measured fluxes within 13-17% in traffic dominated areas. Aerosol fluxes had to be converted from number to mass units, in which a maximum and minimum value for the particle density was applied. The comparison was made with estimates of $PM_{2.5}$ emissions, obtained by scaling down PM_{10} estimates. Total average daily emission estimates in traffic dominated areas were within the estimated upper and lower limit of daily average mass fluxes. In areas dominated by vegetation, estimates of both pollutants were compatible with the measured fluxes within the uncertainty estimate. Overall, results indicated that the local emission inventories are sufficient for many relevant applications.

Contents

Introduction

Anthropogenic emissions of CO_2 and other greenhouse gases are known to induce global warming, and thus expected to have devastating consequences for society in the absence of successful mitigation (IPCC, 2018). Cities are estimated to account for around 75% of global CO_2 emissions (Environment, 2017), where traffic has been observed as the dominant urban source (Velasco and Roth, 2010). Traffic is also a major urban source of aerosol emissions (Conte et al., 2018), that not only lead to severe health effects globally (Brunekreef and Forsberg, 2005; Caiazzo et al., 2013; Mukherjee and Agrawal, 2018), but also represent one of the largest uncertainties in global climate science. Aerosols, or particulate matter (PM), are known to mask global warming effects to an uncertain degree by having a negative radiative forcing, whilst some PM such as black carbon deposits to create light absorbing surfaces with the opposite effect (IPCC, 2013).

Valid estimates of urban emissions on different temporal and spatial scales are crucial for many applications, such as research on the formation of secondary pollutants (Gabusi and Volta, 2005; Gualtieri, 2010), accurate climate models of future scenarios (Stohl et al., 2001), and policy planning or follow-up on mitigation strategies with respect to air quality (Hammarström and Karlsson, 1994; Cloke et al., 1998), and climate (Crippa et al., 2020a). Therefore, as models improve, the need for high resolution urban emission inventories increases. Many cities have established emission databases using a bottom-up approach based on emission factors (EF) (C40 and ICLEI, 2021; HBEFA, 2021). EF relate the rate of emission to some type of activity, for example traffic intensity, emission of a tracer pollutant, or fuel sales, and can be combined with activity data to calculate the emission from a defined region and time period.

Emission inventories have been found to vary greatly between regions, (Zhao et al., 2011; Qiu et al., 2014) even between regional and national level within the same country (Lee et al., 2015), and uncertainties are challenging to estimate (Solazzo et al., 2021). Attempts have therefore been made to evaluate emission estimates by comparing to measured atmospheric concentrations of different pollutants (Brondfield et al., 2012; McKain et al., 2012), local concentrations however do not reflect only local emissions, as they are influenced by long range transport.

The development of the state of the art Eddy Covariance (EC) method has enabled direct measurements of surface emissions, within a limited area. While most frequently implemented for measuring gas exchange over homogeneous landscapes such as forests or agricultural land (Burba, 2013), the EC method has been increasingly implemented in measurement campaigns in urban areas (Feigenwinter et al., 2012). Although most commonly used to study CO_2 emissions (Velasco and Roth, 2010), successful applications for aerosols have been confirmed (Mårtensson et al., 2006; Conte et al., 2018).

Previous studies have derived EF for traffic related aerosols using direct flux measure-

ments, either parameterised by traffic density (Mårtensson et al., 2006; Järvi et al., 2009; Conte and Contini, 2019), or CO_2 emissions (Vogt et al., 2011a). However, the former approach is dependent on a sophisticated estimate of the measurement region, referred to as the footprint, which is hard to obtain for an urban environment. The latter comes with an uncertainty introduced as CO_2 and aerosols do not share all sources and sinks, for example uptake through photosynthesis and and release through human respiration, which are both processes that can have a significant impact on net CO_2 emissions in cities (Moriwaki and Kanda, 2004).

Instead, the approach of comparing model estimates of emissions with direct flux measurements has been taken in a number of studies (e.g. Matese et al., 2009; Christen et al., 2011; Gioli et al., 2015; Stagakis et al., 2019). The successful implementation of this approach, and increased need of validation of modelled emission inventories used as a basis for policy development and climate modelling, has inspired studies where governmental, municipal, or intergovernmental databases of emission inventories are evaluated based on comparisons with EC measurements. In one of the very first studies to attempt such a comparison, Moore et al. (2009) found fluxes of CO_2 and $PM_{2.5}$ to be up 40 times the estimated values based on the local inventory of the State of Kentucky. Lee et al. (2015) studied NO_x emissions in London and found that the national inventory underestimated emissions by on average 80%, while the local city's inventory agreed with measurements within 20%. On the other hand, Marr et al. (2013) found that NO_x emission estimates from the US national emission inventory agreed with EC measurements within 3%. Gioli et al. (2015), when studying CO_2 emissions in Florence, found the annual mean measured emission to be 5% lower than estimates according to the regional inventory, an agreement that was further improved by including local proxies. The large variation in results of these comparisons, between different cities and pollutants, highlight the further need for similar studies in order to reach more accurate emission estimates on all scales, consistent between countries and other regions. However, such comparisons must be done with a lot of caution as applying the EC method in an urban environment is not yet a standardised procedure. There are for instance only recent attempts of developing generalised methods for urban footprint estimation (Auvinen et al., 2017). Furthermore, particularly for the case of aerosols, instrumentation must be chosen with care to make sure that the fluxes measured represent size or mass range that is comparable to what is provided in the emission inventory. Otherwise, fluxes or inventories must be scaled or adapted with caution.

This project features a first comparison between EC measurements and emission estimates in Stockholm and Sweden, and is one of very few where both CO_2 and aerosol fluxes are considered. The measurement site covers a heterogeneous urban area, that can be split into regions with different source characteristics. Bottom-up EF based estimates are retrieved from the emission database of Stockholm Luft- och Bulleranalys (SLB), the department of environmental air and noise pollution at Stockholm Municipality, who provide emission inventories used for air quality management and evaluation of climate targets (SLB-analys, 2021). Furthermore, the EC data used was obtained during a campaign that was carried out a decade ago, with other objectives (Vogt et al., 2011b,a). This study is therefore a demonstration in how a comparison may be conducted using previously sampled data, which could be useful to allow a further increase in emission inventory evaluation, as setting up new EC systems is costly. The aim of this study is therefore to develop a method to allow a fair comparison between emission estimates and existing data from direct flux measurements of CO_2 and aerosols and highlight the

key uncertainties involved. In doing so this thesis aims to answer the research question; To what extent do direct flux measurements of CO_2 and aerosols in urban Stockholm agree with emission estimates based on the bottom-up inventories referenced in local environmental regulation?

Methods

2.1 Eddy Covariance

2.1.1 Theory and concept

The concept of the Eddy covariance (EC) method is quite simple. A turbulent flow consists of 3-dimensional circular movements of air, referred to as eddies, which have large variations in size and frequency. The difference in the number of molecules moving upward with an eddy at a certain time and then downward at another time, will give the vertical flux over a determined time period. Mathematically, this can be expressed as a covariance between vertical wind speed and the concentration of the gas or particle measured.

$$F = \overline{\rho_a w s} \tag{2.1}$$

For gases, this relation is shown in equation 1. The vertical flux is the mean product of the density of the air (ρ_a), vertical wind speed (w), and the mixing ratio of the gas of interest (s). In this context, mixing ratio is defined as the mole fraction in dry air, i.e the number of moles of the gas, divided by the number of moles of dry mixture of the air and gas. As the mean product in equation 1 cannot be measured directly, a couple of important assumptions are made to derive the conventional EC method (Burba, 2013). First, the product is decomposed in the sense that ρ_a, w and s are broken up into a sum of their mean value, over some defined time interval (half an hour in our case), and the instantaneous deviation from that mean at a given point in time. This results in equation 2.2.

$$F = \overline{(\overline{\rho_a} + \rho_a')(\overline{w} + w')(\overline{s} + s')} \tag{2.2}$$

Moving on to expand the parenthesis:

$$F = \overline{(\overline{\rho_a}\,\overline{w}\,\overline{s} + \overline{\rho_a}\,\overline{w}\,s' + \overline{\rho_a}w'\overline{s} + \overline{\rho_a}w's' + \rho_a'\overline{w}\,\overline{s} + \rho_a'\overline{w}s' + \rho_a'w'\overline{s} + \rho_a'w's')} \tag{2.3}$$

The cancelled out terms in equation 3 all correspond to an averaged deviation from the mean, which is zero by definition. Note also that the expression could also be averaged term by term, where the mean values can be moved outside each sum. This simplification yields:

$$F = \overline{\rho_a}\,\overline{w}\,\overline{s} + \overline{\rho_a}\,\overline{w's'} + \overline{w}\,\overline{\rho_a's'} + \overline{\rho_a'w'}\,\overline{s} + \overline{\rho_a'w's'} \tag{2.4}$$

At this stage two major assumption are made. (Burba, 2013) Firstly, all fluctuations in the air density are taken to be negligible compared to the gas flux. This assumption rarely holds when using open path instrumentation, however it can be corrected for which is elaborated on in section 2.3. Secondly, the mean vertical flow (the first term in equation

4) is also assumed to be negligible. The flatter and more homogeneous the surrounding area, the better this assumptions holds. That implies that it does not necessarily hold for all urban environments, but the validity of applying the EC method at the current site has been verified in previous work (Mårtensson et al., 2006; Vogt et al., 2011b). This is also corrected for by a coordinate rotation of the 3D wind components, before the flux calculation. Finally, removing the negligible terms leaves the expression for the flux that can be calculated based on EC measurements:

$$F \approx \overline{\rho_a} \overline{w's'} \tag{2.5}$$

This derivation was done for measuring the flux of a gas, in the case of aerosols it is very similar but using the number density or mass instead of the mixing ratio (e.g. Mårtensson et al., 2006). Note also that a turbulent flow was assumed from the start, which will generally hold as long as measurements are within the inertial sub-layer where turbulence is predominantly driven by wind sheer. However, during nighttime the atmospheric conditions are often more stable, as the surface is no longer heated by solar radiation, minimising convection. At low wind speeds and without convection driven turbulence, the surface boundary layer shrinks. Occasionally it will shrink to the extent where the inertial sub-layer ends up below the measurement tower, so that fluxes are trapped underneath, or transported away by advection, and thus going undetected. Under such conditions, the range of the measurement area can grow by an order of magnitude and no longer represent the area of interest. This issue is commonly dealt with by setting a lower limit for the friction velocity (denoted U*), which is the covariance between vertical and horizontal wind speed and therefore a measure of turbulence.

2.1.2 Footprint estimation

Another important assumption made when using EC, is that the fetch of the measuring station is dominated by the area of interest. That is, that the gas or aerosols in the air parcels that reach the instruments originate from the source area (footprint) of interest, and that the measured concentrations aren't diluted by air from a different type of terrain or exaggerated because other sources lie within the range of the instrumentation.

Conceptually, the easiest way to think about the footprint is that it is what the instrument "sees". It is crucial to the validity of the experiment, but it is not straightforward to calculate. Naturally, the footprint will always cover an area upwind of the measuring station, which means that it moves with changing wind direction, and speed. Furthermore, it's size is affected by the height at which the instrumentation is mounted, the atmospheric conditions, and the topography of the surface that is measured. The heterogeneity of urban surfaces therefore further complicates the process of estimating the footprint, and comprehensive attempts to do so are very rare. To date there is seemingly only one generalised method of estimating urban EC footprints developed, by Auvinen et al. (2017), and the challenge of adapting it to the relevant site lay beyond the scope of this project. However, the findings of Auvinen et al. (2017) suggest that distance from the measurement station to the area of maximum contribution to the footprint can be approximated using more conventional footprint models for homogeneous surfaces, such as the one by Kljun et al. (2015). Early versions of this model were used in previous studies using EC in the same site (Mårtensson et al., 2006; Vogt et al., 2011b).

In this project the model by Hadden and Grelle (2017) was used to visualise and estimate the scope of the footprint. The model computes a radial distance to an area

with the greatest contribution to each half hour flux measurement based on stability, measurement height above the surface, and surface roughness. In this study, the height and surface roughness are assumed to be the same in all directions in the model, which is a crude simplification. Combining all computed distances with flux measurements creates a source flux matrix that can then be overlaid on a map. The R analysis package Openair by Carslaw and Ropkins (2012) was used to plot the matrix (see figure 3.2,3.3. Using the software the modelled distances were binned and combined with the median half hour flux value within each bin, and a smoothing function applied creating a plot with high readability. The median flux value was chosen as turbulent fluxes can contain very large short term variation. The spread in the values contributing to the mean within each bin was not reflected, so the median was assumed to be more representative of the flux.

Randomly selected single footprint calculations were also made with Kljun et al. (2015) to verify the approximate size of the main measurement region. Although none of these models were developed for the complex urban surface, this method can give an indication of the size of an area within which the flux data is representative of the known sources of emissions. A rough approximation of the flux source area was assumed to be sufficient for the data application in this project, further motivated in section 2.7.

2.2   Site and instrumentation

Figure 2.1: Map of the area surrounding the tower where EC instrumentation was mounted

The EC data analysed in this project was gathered during a previous measurement campaign in 2008-2009 by (Vogt et al., 2011b). The EC system was mounted at the top of Hammarby tower (Kalmgatan 37A) in Stockholm, at a height of approximately 120 meters above sea level. Figure 2.1 shows a map of the surrounding heterogeneous landscape. The region north of the tower is closest to the city centre, featuring densely populated areas and large roads, and only fractions of vegetated areas in the form of parks. About 250 meters east of the tower, there is the mouth of a tunnel entered by around 30,000 vehicles per day. To the north of the tunnel there are roads with an average of 6,000-10,000 vehicles per day, and the road furthest to the east is travelled by over 30,000 vehicles per day. In the north west the traffic is dominated by two bridges, together carrying over 40,000 vehicles per day. The larger of the two roads enters a tunnel

north of the bridge, leaving the highest traffic density on roads in this region at around 10,000 vehicles per day.

South of the tower there is one dominant road, located 900m southwest of the tower and heading south, with an average traffic density of around 40,000 vehicles per day. Next to the road there is an entertainment area with arenas, shops and restaurants. The surrounding area east and west of the road is dominated by residential buildings, with vegetation and smaller roads incorporated in between.

To the east-southeast of the tower, there is nature reserve dominated by forest that transitions into a residential area towards the south. There are no large roads, or known significant point sources of emission of the pollutants studied in this project, in this region.

The EC system measurement set-up included the following instrumentation:

- An R3 ultrasonic anemometer from Gill instruments, used to measure wind speed, three-dimensional wind direction and air temperature, which was logged at a frequency of 20Hz

- An LI-7500 open path infrared gas analyser from Licor, used to measure CO2 and H2O concentration at 20Hz

- An optical particle counter (OPC) from GRIMM (Model, 1.109) used to measure aerosol concentration size resolved in 15 channels to a total size range of 250 nm- 2.5 μm, at 1 Hz. It was operated with a dilution unit that mixed sampled air 1:1 with dry (0% relative humidity), zero particle air, resulting in a reduced relative humidity, with the effect that the aerosol diameters can be close to their dry diameters Vogt et al. (2011b)

2.3   Flux data corrections and errors

Pre-processing of the data that is needed prior to calculating the fluxes, such as coordinate rotation, was done by Vogt et al. (2011a,b). However, the final processed data that was used for the publications was not available during this project, and therefore several stages of post-processing and corrections were still needed in order to obtain high quality EC flux data. Firstly, the WPL correction (Webb et al., 1980) was applied to the CO_2 fluxes. This was necessary because the assumption that air density fluctuations are negligible to the measurement does not hold for open path gas analysers. The corrected flux was calculated according to equation 2.6.

$$F_{c,WPL} = F_c + \left(\frac{M_a}{M_w} \frac{\overline{\rho_{c,mass}}}{\rho_{a,dry}} \right) F_q + \left(1 + \frac{M_a}{M_w} \frac{\overline{\rho_{q,mass}}}{\overline{\rho_{a,dry}}} \right) \frac{\overline{\rho_{c,mol}}}{\overline{T}} F_H \qquad (2.6)$$

The second term accounts for water dilution of the CO_2 concentration caused by water vapour flux, and the last term for thermal expansion of the air caused by heat flux. F_c, F_q and F_H denote the fluxes of CO_2, water vapour, and heat respectively. M_a and M_w are the molar masses of air and water. The density ρ refers to the mass or number of moles per unit of air, c and q representing CO_2 and water vapour and $\overline{\rho_{a,dry}}$ being the mean mass density of dry air. This correction resulted in an average increase in the CO_2 fluxes of around 20%. The WPL correction was not necessary for the aerosol data even though an OPC was used. The air flow was diluted and dried before entering the OPC which has been proven to make the WPL correction invalid Ahlm et al. (2010).

Open path gas analysers also come with the risk that surface heating of the instrument induces a heat flux within the measurement column, causing a negative shift in the measured flux. This issue has been observed to result in measurements of negative fluxes of CO_2, implying an uptake, outside of the growing season and even over completely frozen vegetation (Burba et al., 2008). The effect is the strongest during cold temperatures, low fluxes and stable atmospheric conditions. To correct for it , the temperature of either the instrument surface or the air within the measurement column must be known. These parameters where unavailable during this project, so the possible error induced by instrument heating must be considered. The effect is estimated to range between a maximum of 0.05 mg/ms^{-1} at temperatures around -40°C, no more than 0.01 mg/ms^{-1} at 40°C (Burba, 2013). This is about an order of magnitude lower than the average flux magnitude measured. However, during the measurements the instrument was mounted at an angle of about 20°, which greatly reduces the effect, although to what extent is difficult to estimate and will depend on the ambient wind conditions. As the estimated maximum magnitude of the correction was relatively small to begin with, this effect was considered to be negligible.

The aerosol fluxes have been corrected for tube losses in the 13m long sampling line between the tube inlet and the OPC following Hinds (1999). Particle losses due to Brownian diffusion is negligible in the OPC size range. Most of the tube was oriented vertically, which minimises loss due to gravitational settling, however a small length of tube was horizontal, and curved, resulting in both gravitational losses and impaction. Gravitational losses were estimated for each of the 15 size channels separately. The aerosol fluxes were then unit converted from number to mass, and the tube loss correction led to an average increase in the mass flux of 15%. The relative larger size of the particles in the sampling line prior to the aerosol being dried was not considered due to lack of information of the aerosol hygroscopicity. It may lead to an underestimate of the tube loss correction of a few percentage points. The larger underestimate (correction) presented in this study compared to the 5% reported by Vogt et al. (2011b) for the same sampling line is because aerosol mass fluxes were considered in this project, while Vogt et al. (2011b) reported the correction in aerosol number.

As the OPC has a measurement frequency of 1Hz as opposed the sonic anemometer that measures at 20Hz, turbulence with a higher frequency than 1Hz is not resolved and the fluxes are underestimated. Furthermore, the laminar flow in the sampling line causes signal dampening which has a similar effect. The combined effect has been corrected for according to the method proposed by Horst (1997). The corrected flux F_{corr} is calculated by

$$F_{corr} = F_m \left(1 + \left(\frac{2\pi n_m \tau_c \overline{U}}{z} \right)^\alpha \right) \tag{2.7}$$

where F_m is the measured flux, z is the measurement height and $\overline{U}$ is the half hour mean horizontal wind speed. The first order response time constant τ_c for the Grimm 1.109 was measured by Ahlm et al. (2010) and determined to 0.3s. For the combined instrument and sampling line, Vogt et al. (2011b) estimated a total $\tau_c = 1$s that was applied for this correction. The suitable value for α varies between 1 for during stable stratification, and 7/8 for neutral or unstable. The stratification conditions are obtained by z/L, where L is the Monin-Obukhov length which is the theoretical height where the cause of turbulence is dominated by convection as opposed to wind sheer. When $z/L > 0, z/L = 0$ and $z/L < 0$ correspond respectively to stable, neutral, and unstable stratification. Finally,

n_m is 0.085 when $z/L \leq 0$, and given by

$$n_m = 2 - \frac{1.915}{1 + 0.5\frac{z}{L}} \tag{2.8}$$

when $z/L > 0$. The correction for the limited resolution of the OPC led to an average increase of 12% in the aerosol fluxes.

2.4 Aerosol flux unit conversion

During this project, only the integrated fluxes of aerosols >250nm were considered, and no individual size channels are presented in the results. However, the fluxes for individual channels had to be used to convert the fluxes to units of mass. The unit conversion was necessary as the emission estimates based on EF were only available in mass units. The half hour mean number flux in each channel, dF_N, was converted to mass by equation 2.9.

$$dF_M = dF_N * \frac{4\pi}{3} \left(\frac{D_g}{2}\right)^3 * \rho \tag{2.9}$$

The mass flux is denoted dF_M, D_g is the geometric mean of the upper and lower limit of each size bin, and ρ is the mass density of aerosols. The choice of density is one of the largest sources of uncertainty in the measured aerosol fluxes. Urban aerosol emissions are predominantly traffic induced, but vehicle exhaust particles are mostly smaller than 0.2 μm and thus only marginally detected by the OPC. Therefore, the measured fluxes mainly represent non-exhaust emissions, consisting of emission and re-suspension of brake-, tyre-, and road-wear particles. To reflect the spread in the mass fluxes depending on the choice of density, two densities have been applied. For the lower limit, a value of 0.75 g/cm³ is used, which is the density of brake-wear particles as measured by Nosko and Olofsson (2017). The maximum density of particles in road run-off water found by Kayhanian et al. (2012), 2.2 g/cm³, was used as the upper density limit. The choice of the two densities applied represent the maximum expected range between the mass fluxes, as the lower and upper density choice correspond to fluxes consisting entirely of brake and road wear particles, respectively.

2.5 Flux data processing

Due to instrumentation failures and maintenance issues, there was only CO_2 and aerosol flux data available from 72% and 84%, respectively, of the entire measuring period from April 1st in 2008 to April 7th in 2009. Additional data was removed during data processing. As an open-path gas analyser was used, spikes in the CO_2 flux data were caused when precipitation interfered with the measurement path. Therefore more of the CO_2 data was removed, although a de-spiking regime where spike limits of 20 times the negative and positive median was applied to both CO_2 and aerosol fluxes.

Data from time periods with $U^* < 0.1$ was also removed, to exclude data from periods with too little atmospheric turbulence for valid measurements. For U^* values below 0.1, the fluxes were small and showed a clear increase with U^*, which eventually levelled off towards a higher U^*. Furthermore, fluxes from periods between nautical dusk and dawn,

during which negative CO_2 fluxes were observed, were also removed. These are periods at night where there is no photosynthetic active radiation and thus photosynthesis is not possible. An observed CO_2 uptake therefore indicates an unreliable measurement, or that the sensor is outside the inertial sublayer. After these criteria were applied, CO_2 data for 52% and aerosol data for 63% of the entire measurement period remained.

Flux data corrections, analysis and plotting of the spatial and temporal variation in the flux and wind data was carried out using R version 3.6.3 and data analysis package Openair (Carslaw and Ropkins, 2012).

2.6 Emission estimates

2.6.1 Emission factors

EF relate the rate of emission to the activity directly or indirectly inducing the emission. The emission factors from the Handbook of Emission Factors for Road Transport (HBEFA) are expressed per unit of vehicle activity, and the general formula for calculating emissions based on this type of EF is shown in equation 2.10 (Hickman et al., 1998).

$$Q_i = \sum_{j=1}^{n} \sum_{k=1}^{m} N_{j,k} \cdot e_{i,j,k} \tag{2.10}$$

where Q_i is the emitted amount of pollutant i, e is an EF, N is the amount of traffic, k corresponds to different vehicle types, and j different kinds of vehicle operation. HBEFA contains EF for a range of pollutants, including CO_2 and PM relevant for this project, by all currently operated vehicle types and categories (HBEFA, 2021). For six european countries, including Sweden, HBEFA EF specified for the countries vehicle fleet are available.

2.6.2 SLB emission estimates

The results from the direct flux measurements of CO_2 and aerosols were compared to emission estimates provided by Stockholm Luft- och Bulleranalys (SLB), which is the department of environmental air and noise pollution at Stockholm Municipality. SLB's emission database includes point sources of emissions such as treatment plants and ships, and traffic emissions calculated specifically for each different road type, defined by the fraction of heavy to light duty vehicles, the speed limits, and temporal traffic variation. Vehicle exhaust emission is calculated by combining HBEFA EF for each vehicle type, with traffic activity data. Non-exhaust emissions of PM is calculated using the NORTRIP model by Denby et al. (2013), that takes into account the use of studded tyres, and a surface moisture model. The software Airviro (Airviro, 2021) is used by SLB for organisation and calculations based on the data, and can provide calculated hourly averaged emissions within a selected area and time period.

Traffic activity is a combination of vehicle fleet composition and the traffic flow on a road, which are provided by the Swedish Transport Administration or the local municipality depending on the road type. The traffic flow is updated yearly, based on the hourly average flow of the previous year. Each month is averaged separately, as well as four different day types; Monday-Thursday, Friday, Saturday and Sunday. However, the vehicle fleet composition is updated sporadically, and for this project the composition for

2015 and 2020 was available, combined with the HBEFA EF from the same years. In 2008, when most data for this project was obtained, specific EF for Sweden were not yet included in the HBEFA database. Therefore, for a relevant assessment of the updated HBEFA EF, the 2015 and 2020 scenarios were used to extrapolate to the 2008-2009 scenario. To reduce the number of day types for the comparison, Monday-Friday as well as Saturday-Sunday were averaged together, resulting in one weekend and one weekday set of hourly averages.

CO_2 is one of the pollutants incorporated in the SLB database and it was therefore straightforward to obtain an emission estimate for the comparison. However, emission calculations of aerosols with a dry diameter only in the size range 0.25-2.5 μm as the measured particle flux data, could not be provided. In the mass flux of aerosols, the largest size masses dominate. Therefore, the aerosol size range of the flux measurements is in mass comparable to $PM_{2.5}$. Unfortunately, $PM_{2.5}$ is not incorporated in the SLB emission database either. Instead PM_{10} was used, scaled in order to be comparable to the direct flux measurements of in the relevant size range.

To find the relationship between $PM_{2.5}$ and PM_{10}, measurements of their concentration from a street level urban air quality monitoring station at Hornsgatan in Stockholm were utilised. Note that these are measurements of concentration and not flux, but they were used to estimate non-dimensional scaling factors. Background concentrations, measured at a monitoring station on a rooftop nearby, were removed to reflect only local emissions. As PM_{10} also contains $PM_{2.5}$, linear regression was performed to fit the relation between PM_{10} concentration and the difference in concentration between PM_{10} and $PM_{2.5}$. Each month was fitted separately, to account for seasonal variation, resulting in a monthly scaling factor denoted by α_m. However, there was not enough data available for January, February and March, so $\alpha_{December}$ is used for the former, and α_{April} applied to the two latter.

The linear fit with the monthly variation is shown in figure 2.2, where the slope of each line is α_m. Each fit had an R^2 value between 0.882 and 0.999. To obtain emission estimates of $PM_{2.5}$, the SLB PM_{10} estimates for each month were multiplied by $1 - \alpha_m$.
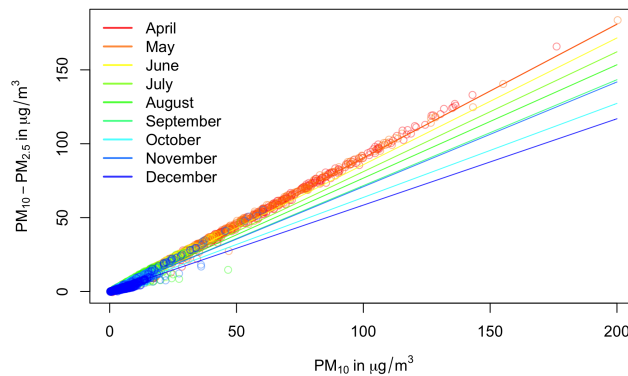
Figure 2.2: The relation between PM_{10} and the difference between PM_{10} and $PM_{2.5}$ concentrations from street-level measurements on Hornsgatan in Stockholm from April to December. Linear regression was performed for each month separately.

2.7   Comparison

Great caution must be taken when comparing EC flux measurements to EF based emission estimates. The EF estimates are calculated for a well defined source area, with a finite number of influential processes accounted for by modelling, and based on monthly averaged activity. The flux measurements on the other hand, capture half hour averages of real world emissions, affected by unlimited atmospheric processes. While the flux source area can be narrowed down greatly compared to when measuring only concentrations, it is not well defined and varies during the measurement period. Therefore, the approach in this project was to attempt to obtain comparable averages, by averaging long term measurements and selecting a suitable spatial scale for the comparison by estimating the average footprint and selecting appropriate sub-areas.

The half hour EC flux measurements are expressed as the mass or amount of pollutant per second and square meter, reflecting the temporal and spatial mean flux from the current source area. As the footprint changes in both size and direction depending on conditions, averaging fluxes over a longer time period will reflect the overall average flux from a larger area. If the area is relatively homogeneous in the distribution and magnitude of emission sources, then the average flux should be comparable to the EF based estimated emissions from any sub-area selected within the average flux source area. If the area is heterogeneous, the sub-area must be of comparable size to the footprint or at least contain approximately the same ratio of key influential sources to areas of low emissions. For areas with very heterogeneous source distribution, for example large areas with low emissions, containing single point sources with high emissions, it is more import that the distribution of wind directions and wind speeds in the flux measurement over that region is even. Otherwise, when the mean flux is used to calculate the total emission from the area, the contribution from the point source could be unrepresented, or completely dominant.

As the tower is surrounded by areas with different types and magnitudes of emission sources, the flux source area was split into four subsectors, the northeastern (NE), southeastern (SE), southwestern (SW), and northwestern (NW) quadrant. The choice of how to split the wind directions was based on the distribution of the different area types in the surroundings as well as the distribution of wind directions, while the size of the sub areas for the comparison was determined using the flux source estimates. The software for selecting the areas for EF emission calculations was limited to rectangular shaped selections, which also influenced the choice of sub sectors. Finally, a size of $1500m * 1500m$ was chosen for the areas, to be large enough to reflect the same source distribution as the footprint, but small enough to fit well within it. The area selections are marked in figures 3.2 and 3.3. The distribution of wind speed and direction over the SW quadrant, as well as the results from the flux source estimates indicated that the footprint was significantly different in size or distance than over the other sectors. Therefore an additional sub-area selection of 3000m*3000m, and subsequent comparison, was made for the SW sector. The measured fluxes in units of mass per m^2 per second were averaged over every hour, as the SLB estimates were of hourly emissions. Then they multiplied with the area selected for the emission estimates, before calculating the mean hourly fluxes for the entire time period. So, the comparison was made between the average hourly measured fluxes, and average hourly emissions estimates within the total area. Weekdays and weekend days were evaluated separately, because of the difference in traffic patterns.

The standard deviation of the mean hourly fluxes is used to represent the uncertainty

14

in the EC measured emissions, as spread in the mean is caused not only by temporal variations, but also the spatial variation of the footprint. In the comparison of CO_2 emissions, this uncertainty is not comparable to the spread in the mean of the SLB estimates, as it only reflects the temporal variation in the traffic activity data. Calculations showed that the spread in the mean SLB estimate of CO_2 emission was consistently less than half the magnitude of the spread in the mean measured data. Therefore, no uncertainty is included for the estimated CO_2 emissions. To asses the extent of agreement in total estimated emission, the hourly averages for the entire year, including weekdays and weekends, were accumulated to equal the mean total daily emission from each sub area. The percentage error in the SLB estimates compared to the direct flux measurements was also calculated.

In the comparison of aerosol emissions, there is uncertainty introduced in the emission estimates by the scaling of PM_{10} to $PM_{2.5}$. As the scaling is done monthly, based on measurements of concentrations rather than models, it will have altered the temporal variation in the emission estimates. Therefore, standard deviation of the mean hourly emission estimates as well as the mean measured fluxes are included in the comparison of aerosol emissions. However, when fluxes are large in magnitude, the biggest uncertainty in the aerosol fluxes is introduced by the conversion from number to mass flux, as the true density is not known. As two densities were used, there are two sets of average hourly fluxes, and two values for the accumulated mean flux. Therefore, the extent of the agreement between emission estimates and flux measurements of aerosols could not be assessed in the same way as in the CO_2 comparison. However, as the chosen densities represent the upper and lower limit for the measured mass fluxes, the spatial and temporal consistency in the agreement could still be assessed to a certain degree.

Results

3.1 Analysis of flux data

3.1.1 Wind distribution
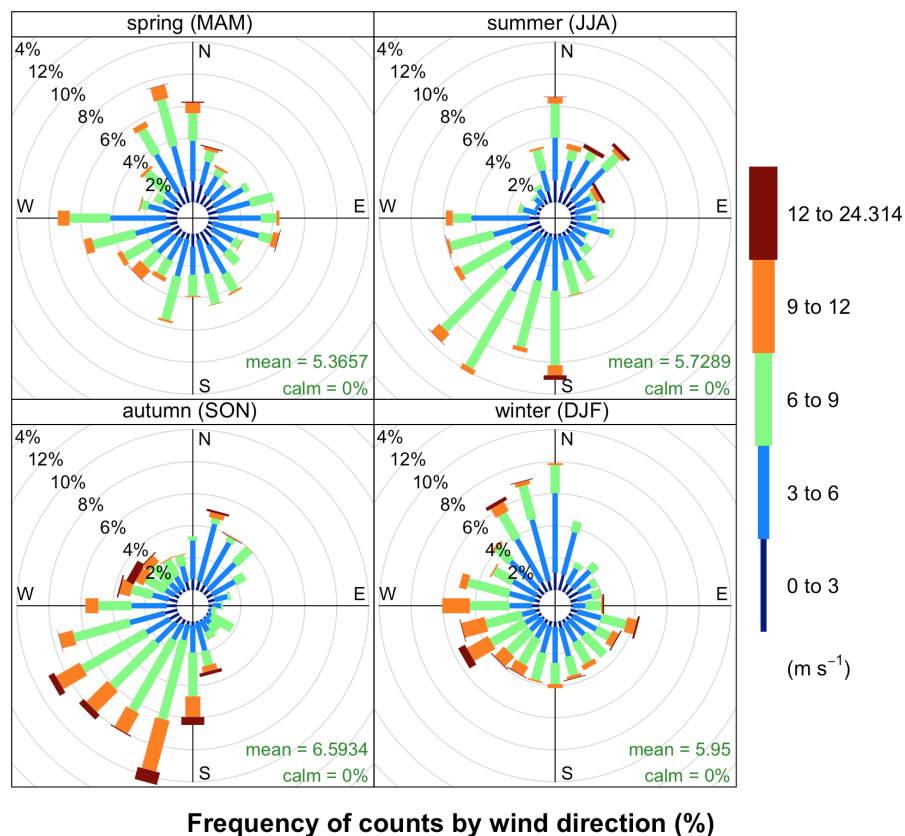
Figure 3.1: Distribution of wind speed and direction by season. Wind speed counts are binned into 15 m/s intervals. The length of each segment represents the percentage frequency of all wind counts that come from the any direction within the current bin.

The distribution of wind directions in the flux data, by season, is displayed in figure 3.1 which also shows the variation in wind speed for each direction. Spring is defined as March to April, summer June-August, autumn September-November, and winter December-February. The most even distribution of wind directions is found in spring. In the winter, the wind is relatively evenly distributed in the south, but not in the north leaving

16

the NE under represented during this season. During summer and autumn the winds are similarly distributed, where SW winds dominate both periods and SE and NW winds are less frequent. During these seasons the wind speeds measured in the SW sector are also significantly higher than in all other sectors. Figure 3.1 also shows that during each season, the distribution of wind directions is relatively even within each quadrant and therefore strengthens the choice of quadrant size selection.

3.1.2 Flux source area

A visualisation of the CO_2 flux source area is plotted figure 3.2 as an overlay over a map of the area, where roads with heavy traffic are distinguishable. The figure reflects the heterogeneity of the source area, and the spatial variation in the fluxes is different between and within the four quadrants, particularly both northern sectors. The flux source area model, although to some extent geographically shifted from reality does show areas of higher emission fluxes with geographical similarities to major road networks. In the north for example, the size and shape of the areas of high fluxes according to the model can be associated with roads with high levels of traffic activity in the area. To the east a large point source is identified in the flux source area analysis. This coincides well with the opening between two tunnels with traffic activity of ca 30,000 vehicles per day. In both southern quadrants, the variation in the flux size is less prominent within each sector. The road with the most traffic in the NW continues down into the SW sector, yet the fluxes are smaller in magnitude, more uniformly distributed, and seem less dominated by one source. However, the area with higher fluxes closest to the tower in the SW could be associated with the large road, assuming the same positional shift as in the north. In the SE sector, positive fluxes are low and fairly evenly distributed, with an area of uptake in the centre. There is no remarkable difference in the fluxes over the park versus the residential area, both included in this sector, as the region where a visible uptake is found according to the model is located over the transition area between the two landscape types.

Figure 3.2: Map of the area surrounding the tower where the EC system is mounted, overlaid with a flux source estimate. The distance to an area of largest contribution to the current footprint was calculated using the method by Hadden and Grelle (2017). Modelled distances have been binned and combined with the normalised median half hour CO_2 flux within each bin, and a smoothing function has been applied. The four square areas in the centre of the plot mark the areas for which the SLB emission estimates have been calculated, and the EC fluxes scaled by, for the comparison between fluxes and estimates.

Figure 3.3 shows the flux source estimate generated using the median aerosol flux instead of CO_2. In the north, the modelled areas of high fluxes clearly coincide with those for CO_2, particularly in the NE, and show even higher relative fluxes. In the NW, the spatial flux distribution is slightly shifted to the east compared to for CO_2, and the area with negative flux is more prominent. In the SW, the spatial variation is very similar to the corresponding sector in figure 3.2, but lower in relative magnitude, unlike both northern sectors. The SE sector stands out by featuring a largely different spatial distribution in the flux source estimate for CO_2 and aerosols. Figure 3.3 shows an area of significant positive flux from the area between 90°-135°, that coincides with the park location. In the other half of the SE sector fluxes vary between positive and negative but stay very low in magnitude, apart from towards the edge of the plot where the negative fluxes of the highest relative magnitude of all four sectors are found.

Figure 3.3: Map of the area surrounding the tower where the EC system is mounted, overlaid with a flux source estimate. The distance to an area of largest contribution to the current footprint was calculated using the method by Hadden and Grelle (2017). Modelled distances have been binned and combined with the normalised median half hour aerosol flux, within each bin, and a smoothing function has been applied. The four square areas in the centre of the plot mark the areas for which the SLB emission estimates have been calculated, and the EC fluxes scaled by, for the comparison between fluxes and estimates.

3.1.3 Temporal variation

Figure 3.4 shows the median diurnal trend by wind direction in the EC measured CO_2 fluxes, plotted separately for the four seasons. For northern wind directions, fluxes peak during daytime throughout all seasons. The SE sector, with the most vegetation, shows a very different trend with near zero or negative fluxes during the day that increase towards the night, which is particularly pronounced in the summer season. The largest positive fluxes in the SE are found in winter during afternoon. A net uptake is detected during mornings in the same season, although there is not enough data from this region and time period to complete the plot. During autumn, fluxes can be seen to peak twice during the day in the SW, NW and SE sectors, at times that can be associated with traffic rush hours. The SW and NW show similar trends in winter, while the emission peak is more constant throughout the day for the other seasons. Both western sectors are also show a very flat diurnal trend in the summer, although missing data data disrupts the figure in the NW. Peak fluxes are highest in the NE sector, consistent with figure 3.4, with the largest values found in spring and autumn. The uptake that can be seen towards the east in the plot spring is likely due to smoothing effects, as all negative night time fluxes of CO_2 have been removed.

The magnitude of median CO_2 fluxes span from -0.4 mgm^{-2}s^{-1} to 1.4 mgm^{-2}s^{-1}.
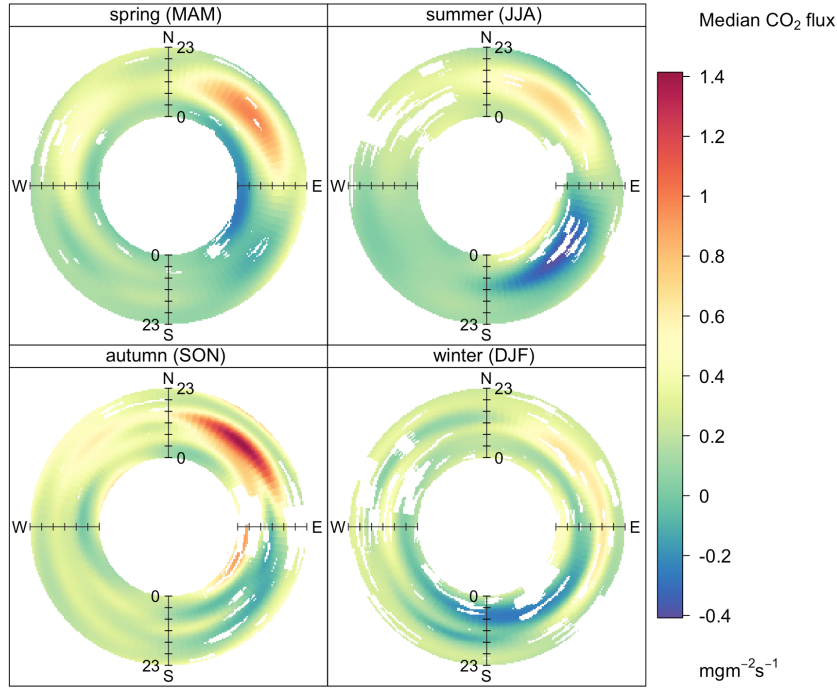
Figure 3.4: Diurnal trend in median EC measured CO_2 fluxes plotted by wind direction, split by season. The axis in the sub plots represent hours, where the edge of the inner circle marks the first hour of the day and the outer edge the last. Wind direction data has been binned into 4° intervals, and a smoothing function applied.

The corresponding plots for the aerosol measurements are displayed in figure 3.5. Here the most prominent seasonal trend is the clear increase in aerosol fluxes during spring, particularly for the northern sectors. Furthermore, fluxes are in the north are consistently positive with a daytime peak during all seasons, although emissions are higher in the NE, especially during the winter season. For most of the SE sector fluxes peak during the day, unlike in the CO_2 trends, with the exception of the south-most region in summer where a daytime deposition is observed. Double daytime peaks, observed in CO_2 the autumn for most sectors, are only distinguishable in aerosol fluxes in the NW sector. The SW shows the flattest diurnal trend of all sectors during all seasons, with the most temporal homogeneity observed in winter.

The magnitude of median mass fluxes of aerosols in the size range 0.25-25μm span from around -0.03 μgm^{-2}s^{-1} to over 0.06 μgm^{-2}s^{-1}.
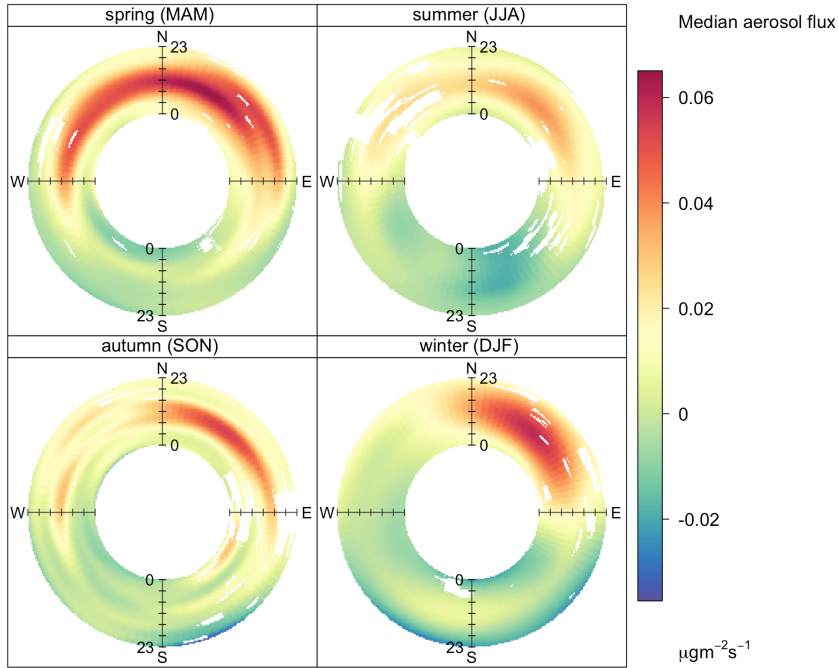
Figure 3.5: Diurnal trend in median EC measured aerosol fluxes plotted by wind direction, split by season. The axis in the sub plots represent hours, where the edge of the inner circle marks the first hour of the day and the outer edge the last. Wind direction data has been binned into 4° intervals, and a smoothing function applied.

3.2 Comparison

3.2.1 CO_2

The average EC measured diurnal cycles of CO_2 flux during weekdays, for the four wind sectors, are plotted in figure 3.6 together with the corresponding average SLB emission cycle estimate. Each sub figure also states the accumulated total flux during an averaged day according to the respective method, and the spread in the flux data represented by the standard deviation of the mean.

In both northern sectors, as well as the SW sector (subfigures (a),(b) and (c)), there is a clear traffic dependence in the measured flux, which is in line with the clearly traffic dominated emission estimates. However, the increase in emissions in the morning, presumably caused by the morning rush in the traffic, is delayed in the flux measurements compared to the estimates. Furthermore, the fluxes are almost consistently higher than the estimated emissions at nighttime, but go down significantly before the morning increase in NW and NE. In the NW the fluxes during the night are higher than the estimate, but lower during midday to afternoon. This could be due to uptake from vegetation, but the accumulated fluxes indicate that it has a negligible contribution to net emissions in this sector. In the NE sector, the fluxes show no significant sign of photosynthesis and are in fact higher than the estimate even in the afternoon.

Overall, the average CO_2 fluxes show a good agreement with the estimates from SLB, especially during daytime. In the northern and SE sectors (subfigures (a),(b) and (d)), the estimates lie within approximately 2σ of the flux measurements with very few exceptions. However, the SW sector stands out. While the temporal trend of the flux

shows the seemingly best agreement to the estimates, the magnitude of the flux during the day, and subsequently the total accumulated flux, is less than 50% of the estimated. Although the accumulated flux in the SE sector is also far off from the estimate, this is less remarkable as the estimated emissions still lie within the uncertainty range for most of the day.
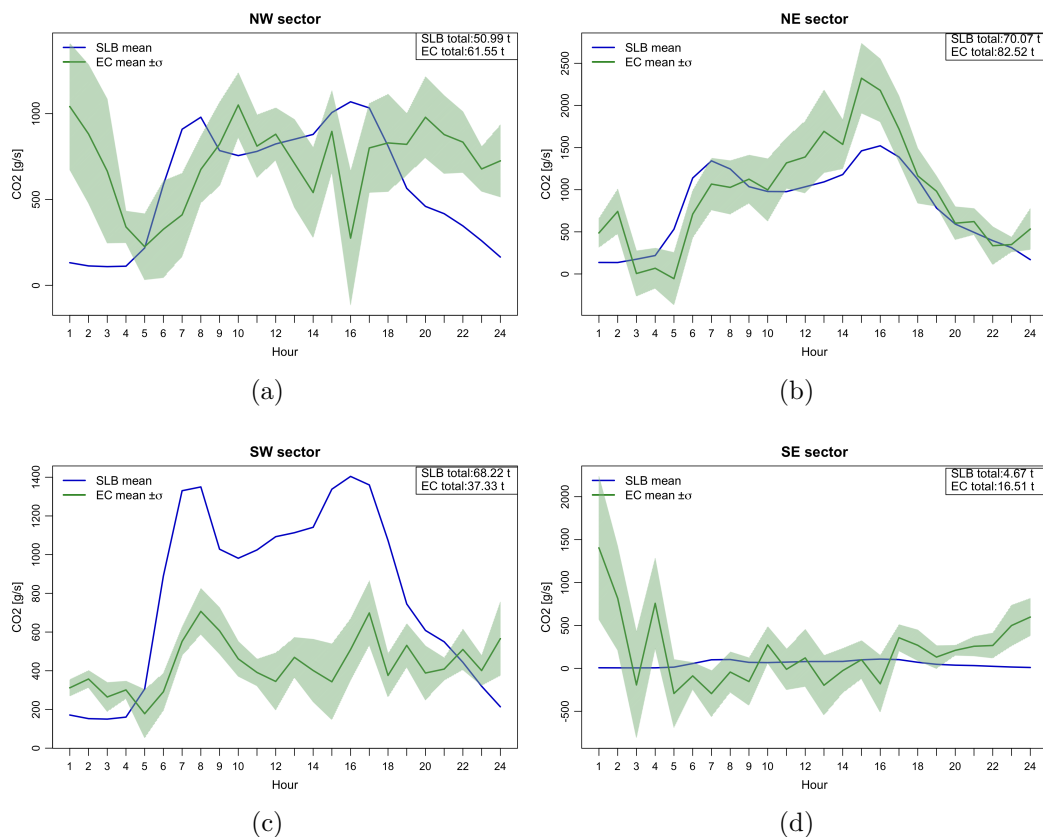
Figure 3.6: EC measured mean diurnal cycles of CO_2 emissions for weekdays between april 2008 and april 2009, plotted with SLB mean emission hourly estimates for the same time period. Shadowed area shows the range of the EC mean $\pm\sigma$, the standard deviation of the mean. Total SLB and EC refer to the total accumulated emission for the average weekday. Subfigures correspond to wind sectors a) North-west, b) North-east, c) South-west, and d) South-east.

The SW sector stands out also in the average diurnal comparison for weekend days, as shown in figure 3.7(c). The midday peak in the estimated emissions, presumably driven by traffic activity, is much less pronounced in the average flux. Both morning peak, afternoon peek and noon fluxes are about a factor 2 smaller than the estimated emissions. All other sectors (figures 3.7(a),(b) and (d)) again show compatibility with the hourly emission estimates, as well as the accumulated flux. Even though the shape of the flux curve in the SE sector is even more decoupled from that of the estimated diurnal curve, showing a trend of uptake during daytime and positive fluxes during the night, the accumulated emissions are much more comparable than during weekdays. In the NW sector, the trend in measured emissions follow the estimates during daytime, but deviates during the night. Although still larger, night time fluxes are more compatible with the estimates than during weekdays, particularly in the evening as the spread in the data grows with the fluxes in figure 3.9(a).

A delay in the daytime increase in emissions is observed in the northern sectors, similarly as for weekdays.
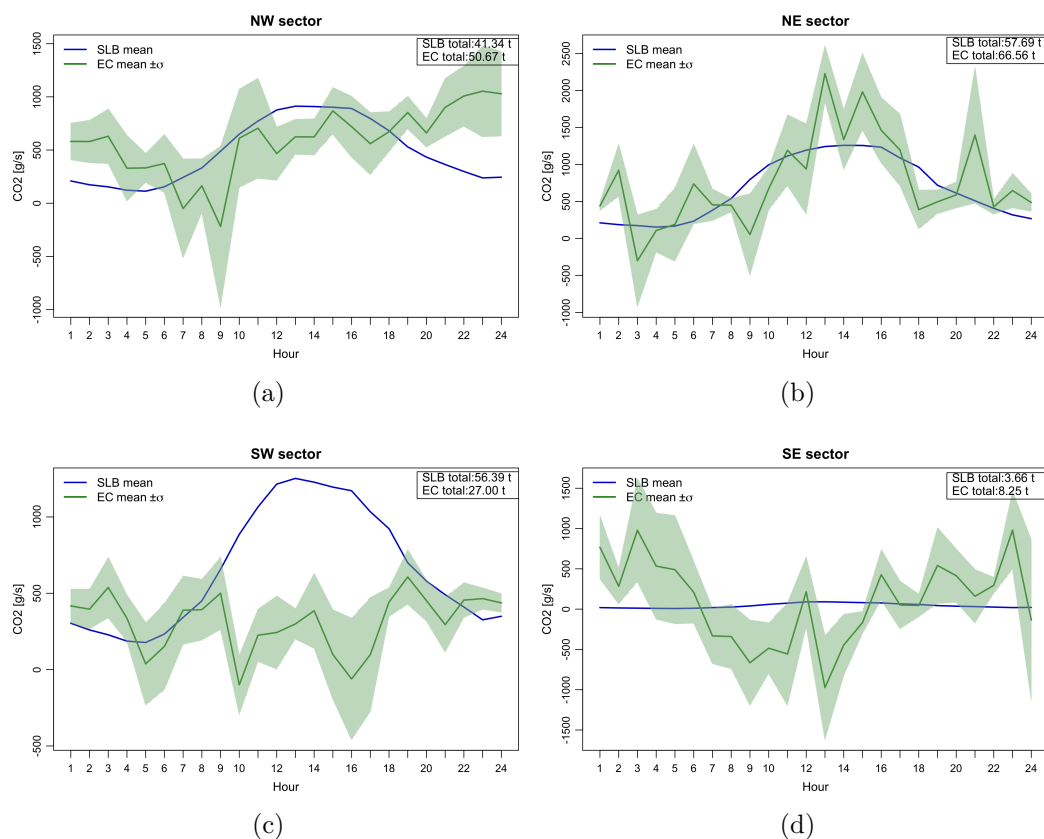
Figure 3.7: EC measured mean diurnal cycles for weekend days between april 2008 and april 2009, plotted with mean hourly emission estimates from SLB's emission inventory for the same time period. Shadowed area shows the range of the EC mean $\pm\sigma$, the standard deviation of the mean. Total SLB and EC refer to the total accumulated emission for the average weekend day. Subfigures correpond to wind sectors a) NW, b) NE, c) SW, and d) SE.

Table 3.1: Table shows the accumulated average hourly averaged emissions, thus the average daily total emission, of CO_2 for both EC measured CO_2 fluxes and emission estimates based on SLB's emission database. Values have been calculated for an area of 1500m∗1500m, located in the NE, SE, SW and NW quadrant with respect to the measurement tower, respectively. Uncertainty in EC values, σ_c, is represented by the standard deviation of the mean. Percentage error is calculated for emission estimates in relation to EC values. Deviation indicates within how many σ_c the SLB total and EC total values agree.

Wind sector	NE	SE	SW	NW
CO_2, EC daily total	77 ± 21 t	14 ± 22 t	34 ± 8.5 t	58 ± 17 t
CO_2 SLB daily total	67 t	4.4 t	65 t	48 t
Percentage error	13%	69%	49%	17%
Deviation	$< 1\sigma_c$	$< 1\sigma_c$	$> 3\sigma_c$	$< 1\sigma_c$

Table 3.1 shows the accumulated hourly estimates and measurements of CO_2 emissions in each sector, averaged over the entire measuring period. The deviation indicates within

23

how many standard deviations (σ) of the mean in the EC value that the SLB value is found. The NW, NE and SE sector all show an agreement well within one σ, even though the percentage error in SE is 69%. In the SW sector however, the agreement is not even within 3σ.

3.2.2 Aerosols

The results of the comparison between average EC measurements and SLB-HBEFA estimates of aerosol emissions on weekdays are shown in figure 3.8, for each wind sector separately. The standard deviation of the mean is included for both measured and estimated emissions, and the measurements are represented by two different curves obtained applying the maximum versus minimum density in the conversion to mass fluxes. The accumulated emission is also calculated for both densities, and stated within each subfigure.

As with CO_2, the best agreement in the diurnal trend between estimate and measurement is observed in the two northern sectors (figures 3.8(a), (b)). However, the measured fluxes peak during midday consistently in all wind sectors, in contrast to both the estimates and the temporal trend in CO_2 weekday fluxes. As for CO_2 the emission estimates deliver a diurnal cycle with a morning peak, and an afternoon peak with a local minimum in between, closely following weekday traffic patterns. The observed EC aerosol mass fluxes instead have, especially in the NE sector, more of a single mid-day peak in the upward fluxes.

In the NW, aerosol fluxes show a peak in the first hour of the diurnal cycle followed by a decrease through the night, similarly to in the corresponding plot for CO_2 (figure 3.6(a)). However, the morning increase is earlier in the measured fluxes than in the estimates, as opposed to the delay seen in the CO_2 comparison. In the NE however, there is a time delay of about an hour in the on set of the increase in aerosol fluxes compared to the estimated emission, consistent with the corresponding sector for CO_2.

In the SE sector, 3.8(d) ,the estimated emissions are very low with almost insignificant spread. Although the measured flux magnitudes are much larger with a lot of diurnal variation, they are compatible with the low flux estimates as the spread is so large.

The SW sector stands out in the same way as with CO_2, the trend in the measurements follow the same shape as in the northern sectors, but the fluxes are significantly lower than the estimated, even though the spread in the estimate is large. Figure 3.8(c) even shows negative net fluxes of PM during the night, as well as negative accumulated fluxes.

In all wind sectors, the estimated emission during weekdays is most comparable to the measured fluxes obtained when applying the lower density value. This is quite consistent in the hourly fluxes, and without exception in the accumulated average emissions.
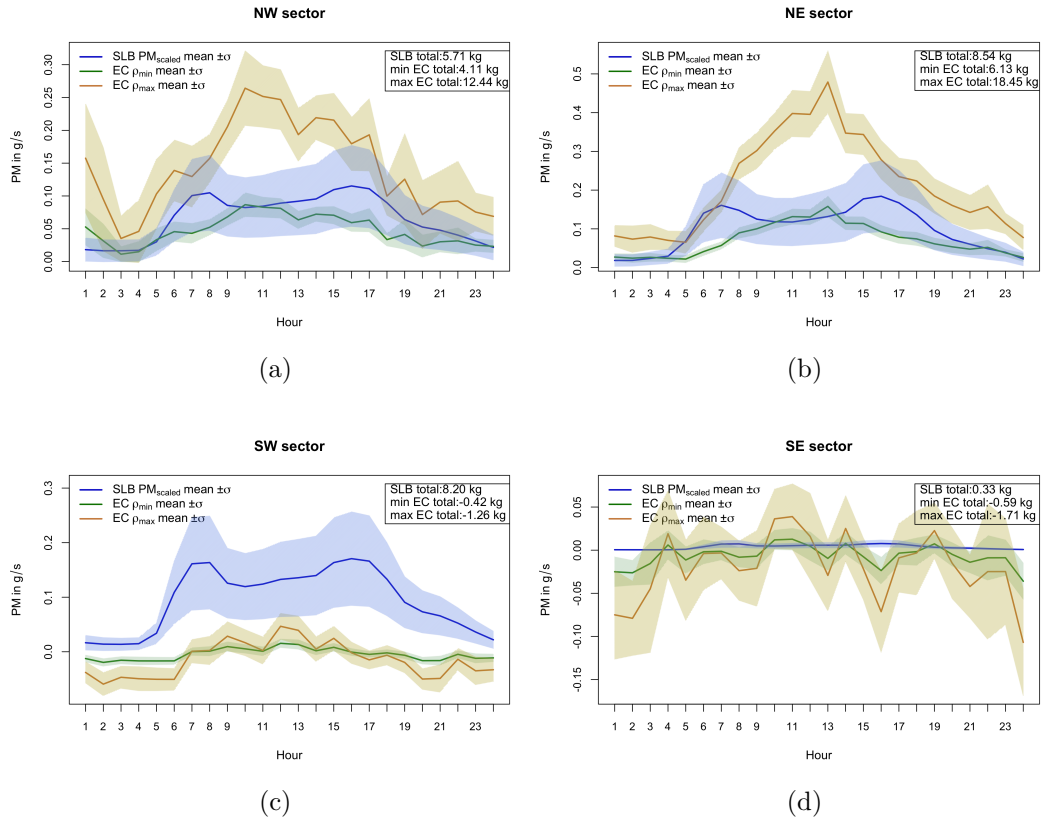
Figure 3.8: Mean diurnal cycles of EC measured fluxes of particles in the size range 0.25-2.5μm for weekdays between april 2008 and april 2009, plotted with mean hourly emission estimates of $PM_{2.5}$, based on SLB's emission inventory for PM_{10}, that have been scaled down (PM_{scaled}). EC fluxes are represented by two different curves, obtained when converting number fluxes to mass and applying a minimum, ρ_{min}, and maximum, ρ_{max}, density. Shadowed areas correspond to the standard deviation of the mean. Total SLB and EC refer to the total accumulated emission for the average weekday. Subfigures correspond to wind sectors a) NW, b) NE, c) SW, and d) SE.

The comparison in average diurnal aerosol emission trends during weekend days are plotted in figure 3.9. In contrast to the result for weekdays, the estimated emissions show the best agreement with the fluxes obtained applying the maximum density in both northern sectors (figures 3.9 (a) and (b)) during daytime, and in the total average emission. During nights however, estimated emissions are low and compatible with the minimum measured fluxes.

In the SW sector, figure 3.9 (c), the average measured fluxes are consistently negative. A peak structure can be seen around 15 pm, temporally coinciding with estimated emissions, but it does not reach higher flux values than during nighttime. Figure 3.9(d) shows average hourly fluxes higher than in the same sector during weekdays, and positive instead of negative accumulated fluxes although still low magnitudes.
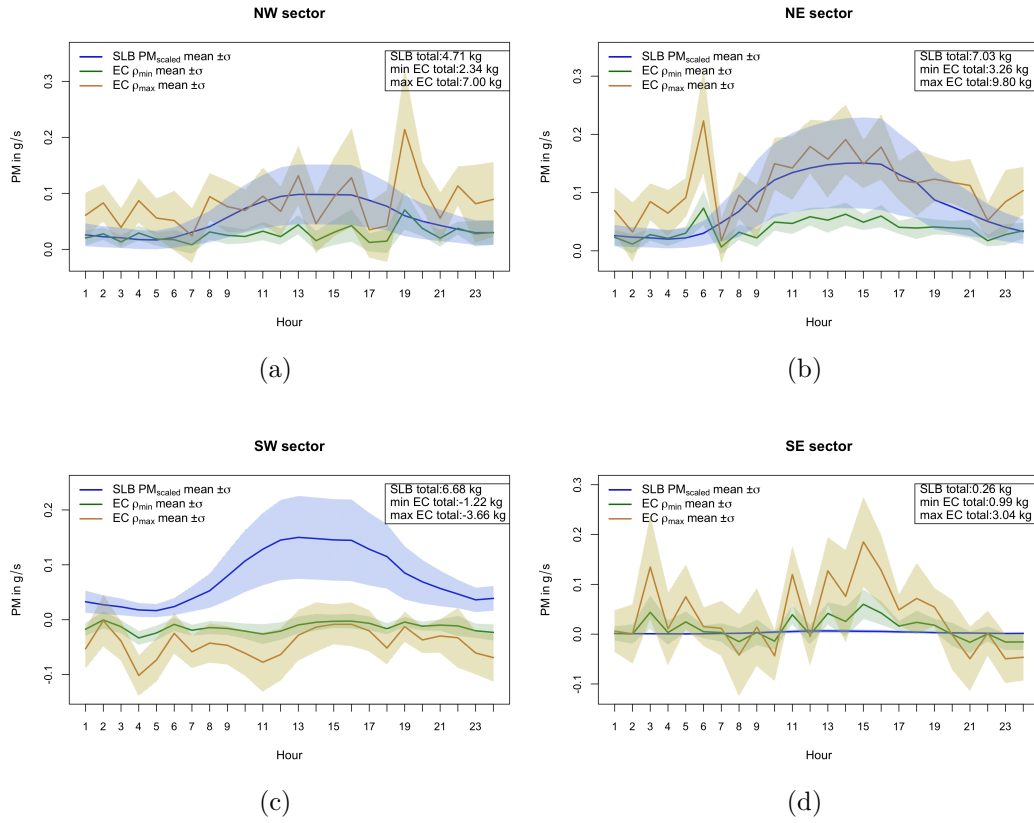
Figure 3.9: Mean diurnal cycles of EC measured fluxes of particles in the size range 0.25-2.5μm for weekend days between april 2008 and april 2009, plotted with mean hourly emission estimates of PM$_{2.5}$, based on SLB's emission inventory for PM$_{10}$, that have been scaled down (PM$_{scaled}$). EC fluxes are represented by two different curves, obtained when converting number fluxes to mass and applying a minimum, ρ_{min}, and maximum, ρ_{max}, density. Shadowed areas correspond to the standard deviation of the mean. Total SLB and EC refer to the total accumulated emission for the average weekday. Subfigures correspond to wind sectors a) NW, b) NE, c) SW, and d) SE.

Table 3.2: Table shows the accumulated average hourly averaged emissions, thus the average daily total emission, of aerosols for both EC measured aerosol fluxes in the size range 0.25-2.5μm and emission estimates of PM$_{2.5}$, obtained by scaling of SLB's emission inventory for PM$_{10}$, that have been scaled down. EC fluxes are represented by two different curves, obtained when converting number fluxes to mass and applying a minimum, ρ_{min}, and maximum, ρ_{max}, density. Uncertainties are represented by the standard deviation of the mean. Values have been calculated for an area of 1500m*1500m, located in the NE, SE, SW and NW quadrant with respect to the measurement tower, respectively.

Wind sector	NE	SE	SW	NW
PM, EC ρ_{min} daily total	5.4 ± 1.0 kg	-0.06 ± 1.2 kg	-0.63 ± 0.54 kg	3.6 ± 1.1 kg
PM, EC ρ_{max} daily total, ρ_{max}	16 ± 3.1 kg	-0.10 ± 3.3 kg	-1.9 ± 1.7 kg	11 ± 3.3 kg
PM, SLB scaled daily total	8.1 ± 4.6 kg	0.3 ± 0.2 kg	7.8 ± 4.4 kg	5.4 ± 3.3 kg

The mean total daily emissions calculated for the SLB emission estimates as well as the two sets of mass fluxes in each sub sector is shown in table 3.2, where uncertainties are represented by the standard deviation of the mean. The uncertainty in the mean

estimates based on SLB data is larger than in the measured fluxes, as can be seen also in the diurnal trends (figures 3.8,3.9). The estimates based on SLB data are consistently most compatible with the mass fluxes obtained when applying the lower density value, ρ_{min}. In the NE,NW and SE sectors the agreement is within one standard deviation of the estimates. In the NE and SE the estimated value also lies between the upper and lower limit of the mass fluxes.

3.2.3   Additional comparison in SW sub sector

The results of comparisons between measured and estimated emissions of CO_2 and aerosols during weekdays from an area 4 times the size (3km*3km) used in the previous comparisons, in the SW quadrant, are shown in figure 3.10. The comparison of CO_2 emissions shows a much better agreement in accumulated average fluxes than with the smaller area selection (see figure 3.6). The magnitude of the two daytime peaks are very similar in estimated and measured emissions. However fluxes are significantly higher during the night, and lower during midday although less notably as the spread is larger.

In the comparison of aerosol fluxes, the agreement in the accumulated values is worse than when the smaller area was selected (see figure 3.8). The estimated and measured emissions are most compatible during midday, when the uncertainties overlap, but as aerosol fluxes are negative during most of the day, the increased scaling of the fluxes from applying larger area selection only causes further deviation from the estimates.

(a)   (b)
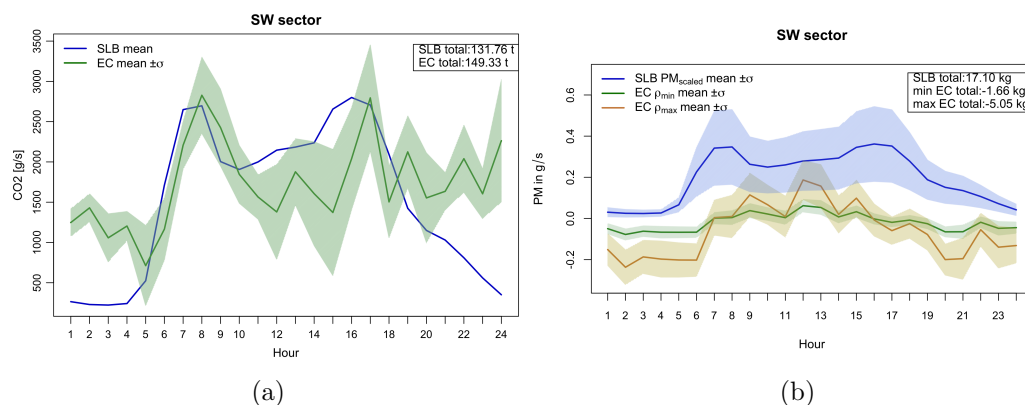
Figure 3.10: Mean EC measured hourly fluxes for weekdays between april 2008 and april 2009, plotted with SLB mean emission hourly estimates for the same time period, over an area of the size 3000m∗3000m in the SW quadrant with respect to the measurement tower. Total SLB and EC refer to the total accumulated emission for the average weekday. Sub-figure (a) shows CO_2 emissions, where the shaded area corresponds the standard deviation of the mean EC measured CO_2 fluxes. Sub-figure (b) shows aerosol emissions, EC fluxes are here represented by two different curves, obtained when converting number fluxes to mass and applying a minimum, ρ_{min}, and maximum, ρ_{max}, density. SlB PM_{scaled} corresponds to emission estimates of $PM_{2.5}$, obtained by scaling down SLB's emission inventory for PM_{10}. Shaded regions correspond to the standard deviation of the mean.

Discussion and conclusions

4.1 Method of comparison and errors in the SW sub-sector

The statistical argument for an estimate of the average footprint being sufficient for the selection of a sub area for comparison was based on the assumption that sources were relatively evenly distributed, or at least represented at equal scale within the sub area and footprint. The distribution of wind directions (figure 3.1) indicated that this could hold within each quadrant, but the variation in wind speed and the flux source estimates both suggested that the average footprint in the SW differed in size or location compared to the other sectors (see figures 3.1, 3.2, 3.3). In both northern sectors the spatial and temporal distribution of fluxes indicate a traffic dependence that can be associated with the large roads in the area. The SW sector contains a road of comparable size and traffic density, demonstrated by the estimated emission in this sector, so the relatively homogeneous spatial and temporal trend in the fluxes from this region indicate that the road is not properly represented. As the fraction of higher wind speed is clearly larger in the SW compared to the other sectors, the average footprint could extend much further. High wind speeds can also result in smaller footprints, but in this case that would imply the fetch is smaller than 900m which seems unlikely, as previous studies measuring at a height a factor three to four times lower have estimated footprints around this size (e.g. Christen et al., 2011; Gioli et al., 2015). It could also simply be that the size of the footprint area is similar to the other regions, but that area of highest contribution to the footprint is shifted further away or closer due two the different wind speed distribution and topography of the area, so that the contribution from the road is underrepresented. Either way, the underlying assumption in the statistical argument fails.

This would explain the disagreement in estimated and measured emissions of both pollutants in this sector. Another possible explanation would be due to an overestimation of the traffic emissions in the calculation via SLB. But this seems highly unlikely, simply because the agreement is so much better in the northern sectors, which are traffic dominated. It is also not likely that it is explained by that CO_2 uptake and particle deposition is not accounted for in the estimates. That would imply that the CO_2 uptake is much larger in this sector than in the SE, which is highly unlikely as it contains far less vegetation. Furthermore, the offset in fluxes due to particle deposition should be of the same scale in other sectors, which is not the case.

To investigate this a test was made by selecting an extended area of 3000m by 3000m, and comparing the new estimated emissions with the scaled fluxes. While the CO_2 fluxes arguably are in much better agreement with the estimate, the agreement in aerosol emissions worsened rather than improved, mainly because the measured fluxes were mostly

negative. The clear double peak in CO_2 mean weekday fluxes indicate that the fluxes are influenced by traffic patterns, but not to the extent of the northern sectors, in the smaller area selection. Aerosol fluxes being largely negative, is also an indication that the footprint cover a large area of vegetation or residential areas, as aerosol fluxes are similar in the SE sector (see figure 3.8(d)).The high CO_2 fluxes at night, and the relatively low fluxes during midday could indicate that significant uptake through photosynthesis and respiration during nighttime is occurring. However, the seasonal variation in the diurnal trend of CO_2 (figure 3.4), show that negative fluxes during midday are observed primarily in the winter, thus more likely to be caused by measurement error than photosynthesis. Hence the low CO_2 during midday in the SW could be influenced by this artefact.

In conclusion, as the size of the region within which the measured fluxes reflect the known sources in the area could not be confirmed in the SW sector based on the flux source area estimate (figures 3.4 and 3.5), the chosen method of comparison is not suitable for this region. Although the agreement between measured flux and estimate of CO_2 emission improved with the second area selection, conclusions on the agreement can not be drawn as it is not known whether the area for which the emission estimates were calculated is comparable to the true footprint. To assess the agreement between measurements and estimates in the SW, the footprint must be estimated more exactly, using a model adapted for urban heterogeneous areas. This result highlights the importance of the development and implementation of such models, to allow future more detailed comparisons.

The method of comparison applied in this project, comparing average daily emissions over an area selected based on simplified estimates of the flux source area, results in relatively high uncertainties in the flux values as it reflects the spread caused by daily, seasonal (as seen in figures 3.4 and 3.5), and spatial variation. Therefore this method is perhaps most suitable for initial comparisons of fluxes and modelled emission estimates, and could likely be used to assess emission inventories with lower resolution such as the EDGAR emission database (Crippa et al., 2020b).

4.2 Comparison of CO_2 emissions

The range of median CO_2 fluxes, -0.4 mgm^{-2}s^{-1} to 1.4 mgm^{-2}s^{-1} as shown in figure 3.4, is comparable to the average range obtained in other EC studies over urban areas, such as Grimmond et al. (2002) who report a range from -1 mgm^{-2}s^{-1} to 1.7 mgm^{-2}s^{-1} in Chicago. In the seasonal variation, opposite diurnal trends were observed during the growing season between the northern traffic dominated sector and the highly vegetated SE sector, indicating that fluxes in the SE are dominated by ecosystem functioning. Considering the average diurnal trends (figures 3.6(d) and 3.7(d)) however, uptake during the day is most likely offset by traffic emissions while weekend fluxes show more typical patterns of ecosystem exchange. The accumulated average flux from this region, presented in table 3.1 is still positive, and larger than the accumulated estimated emission, although with a very large spread. These results indicate that the vegetation in the area is not a net sink of CO_2, and that the gross uptake through photosynthesis is counteracted by the gross respiration. Similar results are found in urban studies such as Christen et al. (2011), whilst even primary and managed forests have been found to act as net sources of CO_2 to the atmosphere (Hadden and Grelle, 2017).

The delay observed in CO_2 fluxes in the traffic dominated sectors during weekday and weekend mornings (see figures 3.6(a),(b) and (c)) could be due to atmospheric effects,

that the inertial sub-layer shrinks below the measurement tower during calm nights. As emissions then can't reach the sensor, this would result in low fluxes during night that increase in the morning when turbulence is initiated by the suns warming of the surface, which will coincide with increasing traffic a significant part of the year. If this were the case and emissions were trapped underneath the sub-layer boundary, there would be a large peak following the onset of turbulence, as emissions accumulated during the night would finally reach the sensor. However, the morning peak is of the same magnitude or, in the case of the north-eastern sector, much smaller than the afternoon peak, and consistently lower than the SLB estimate. Additionally, a strong peak should be seen in the vegetation dominated SE sector as well, as respiration fluxes of CO_2 would build up during the night. Instead the morning peak is absent, and fluxes highest at nighttime. This is not conclusive however, as the spread in the mean, especially during the night, is very high. The absence of a morning peak could be because nighttime emissions are instead transported away via advection and therefore go undetected. However, nighttime fluxes are actually quite high, particularly in the NW, although the uncertainty is also very large and decreases with the flux towards morning. In the plot showing seasonal variation, figure 3.4, a high flux around midnight is only observed in autumn, where wind counts from the NE are quite few (see figure 3.1). The peak in nighttime fluxes seen in around midnight in figures 3.6(a) and 3.6(a) is therefore likely not representative of the average annual nighttime trend, but affected by high flux outliers.

In the NE sector (figure 3.6(b)), the agreement in the average diurnal trend was good during both weekdays and weekends, with a consistent slight underestimation in the SLB estimates compared to measured fluxes in the afternoon. The accumulated mean daily emissions agreed accordingly, with an total underestimate of 13% compared to measured fluxes (see table 3.1). However, as this agreement was well within the uncertainty estimated for the total EC flux, the underestimate was not significant.

A similar agreement was observed in the NW sector, with a 17% underestimate in the accumulated mean SLB estimates, also within the uncertainty range. The agreement in the diurnal trends was slightly different, where fluxes were lower than the estimates during midday, but significantly higher at night. This could be due to photosynthetic uptake in this region, however, the seasonal variation (figure 3.4) shows that measured midday fluxes were low to negative during winter in this sector, which is likely a measurement error that could be effecting the result.

The agreement between measured fluxes and emission estimates in the two traffic dominated sectors is considerably better than initial comparisons made with top-down regional inventories (Moore et al., 2009), and comparable to the agreement of 5 to 15% observed when comparing fluxes to local bottom-up models

4.3 Comparison of aerosol emissions

In the analysis of seasonal variation in the diurnal cycles of aerosol fluxes, there was a distinct increase in fluxes during spring, as shown in figure 3.5. This trend is observed yearly in monitoring of PM_{10} and $PM_{2.5}$ concentrations in Stockholm (Norman and Johansson, 2006), and was explicitly analysed by Vogt et al. (2011b).

The disagreement in shape of the average diurnal trend in PM emissions between the EC measurents and SLB estimates is significant as the shape of the curve is not affected by any of the scalings of the estimate or the choice of density. The delay of the first peak

during weekdays in the EC data could possibly be explained by the previously mentioned atmospheric effects, but not the complete absence of the second peak. Furthermore, when Vogt et al. (2011a) compared diurnal cycles of CO_2 to aerosol number flux in the entire region north of the tower, using the same data, they were found to correlate very well.

The strong midday peak is therefore likely related to the conversion to mass flux. It could be that the distribution of particles varies throughout the day, for instance that lower driving speeds in rush hour produces less road, tyre and brake wear that is the dominant source of traffic induced aerosol mass fluxes. This would imply that driving patterns are not sufficiently accounted for in the EF. It could also be due to that the number of heavy duty vehicles increase during midday as observed by Mårtensson et al. (2006). However, this heavy duty to light duty vehicle fraction is estimated separately for every road and day type, and therefore less likely not to be sufficiently represented. The midday peak could also be caused by a diurnal variation in density. Liu et al. (2015) observed $PM_{2.5}$ densities to be up to nearly 15% higher during midday compared to rush hours, and seasonal variations of similar magnitudes, when measuring concentrations in Beijing. Whilst the variation may partly be explained by a varying mass fraction of soot particles emitted from coal combustion for heating purposes, which is not a significant source in Stockholm, it is also believed to be caused by other processes like secondary particle formation. Hourly monitoring data of $PM_{2.5}$ number and mass concentrations could be used to investigate the density variation in Stockholm in order to asses the impact on the diurnal cycle of the fluxes.

It should be mentioned regarding the comparison in aerosol emissions, that it is likely that the diurnal trend in the emission estimates is more correlated to street level concentrations of $PM_{2.5}$, because of the proximity to the source, and therefore more relevant for air quality applications. However, the results of this study indicate that net mass flux reaching above the urban canopy does not follow the trend of weekday traffic activity.

In both northern, traffic-dominated regions, the estimated emissions showed a closer agreement with the lower density measured fluxes during weekdays (see figures 3.8(a) and (b)), but the opposite during weekends (see figures 3.9(a) and (b)). While the true density should lie somewhere between the two values, this still indicates either an underestimation of emissions during weekdays, or an overestimation during weekends. Previous studies estimating the density of $PM_{2.5}$ have found values between 1.3 and 1.8 g/cm^3 Gao et al. (2007); Liu et al. (2015), suggesting that it is an underestimation during weekends. However, it can not be ruled out that this discrepancy is caused or influenced by the scaling of PM_{10} estimates to $PM_{2.5}$. In future studies, if aerosol flux measurements of particles up to 10μm in diameter are carried out, this effect can be investigated further.

It should be highlighted that net aerosol flux measurements obtained from the eddy covariance technique are a product of the net difference between total emissions and deposition. Particle deposition is not however accounted for in the emission estimates. In a strong source region such as a city with a lot of road traffic, the emission fluxes are about two orders of magnitudes larger than the deposition fluxes (Mårtensson et al., 2006), which is why there was no significant offset observed in the aersol fluxes in the traffic dominated regions compared to the emission estimates. However, in the SE sector, accumulated daily average emissions were negative (see table 3.2), as average hourly fluxes were predominantly negative during weekdays (figure 3.8(d)), and low upward hourly fluxes were observed during weekends (figure 3.9(d)). This reflects the lack of significant sources in this area, as deposition can then occasionally dominate the net fluxes which is also observed in other EC studies of particles in a similar size range (Moore et al., 2009).

However, emission estimates are still compatible with both values for the aerosol mass flux, indicating within this particle size range, deposition fluxes are on average not more significant than emission even within the vegetation dominated SE sector.

The total daily average of the estimated emissions in the northern sector, shown in table 3.2, consistently lay within the higher and lower value for the accumulated mass flux, despite the discrepancy in the diurnal trend. This is the best assessment of the agreement within the limitations of this method, and an indication that the magnitude of estimated emissions likely has a good agreement with total fluxes in the traffic dominated region. However, to improve the accuracy of the comparison, measurements of a size range, and in a unit, more compatible with those of the available emission estimates of particles must be made.

4.4 Summary of main conclusions

A method for comparing previously measured EC fluxes of CO_2 and aerosols to emission estimates based on SLB's emission database was developed. It was applied successfully to three out of four defined sub-areas for comparison. The results in the last sub sector indicated that the flux footprint was not comparable to the area for which estimated emissions were calculated. This result highlighted the main weakness of the method, that the size and spatial distribution of the footprint over time, and the significant sources within the fetch, must be relatively even.

A key issue in this project was the incompatibility of the particle flux measurements and the available estimates of particle emissions. Unit conversion to mass flux and scaling of PM_{10} to $PM_{2.5}$ estimates introduces major uncertainties. The extent of the agreement between estimated and measured fluxes of aerosols could therefore not be quantified to a high degree of certainty. What can be deduced from the results is that within in traffic dominated areas, the estimated emission was within the range of measured fluxes, and most compatible with the mass flux obtained when applying the estimated minimum density. Furthermore, the diurnal trend in aerosol fluxes showed a significant difference in peak structure than the estimates during weekdays. Most probable explanations are that driving patterns have a more significant impact on the mass emissions of particles in the relevant size range than accounted for in EF based estimates, or an unconsidered diurnal variation in particle density.

Average daily total emission of CO_2 estimated using SLBs emission database featuring HBEFA emission factors was found to be within 13 % to 17 % of average daily direct flux measurements in traffic dominated areas. This agreement was within one standard deviation of the measured values.

This project featured an initial comparison between EC flux measurements and emission estimates from SLB. The relatively good agreement found between two so widely different ways to quantify emissions is a strong result, and to some extent a validation of both methods. It is also an indication that local bottom-up emission inventories are sufficient for many applications in climate research and development of mitigation strategies.

Acknowledgements

Bibliography

Ahlm, L., Krejci, R., Nilsson, E. D., Mårtensson, E. M., Vogt, M., and Artaxo, P. (2010). Emission and dry deposition of accumulation mode particles in the Amazon Basin. *Atmospheric Chemistry and Physics*, 10(21):10237–10253.

Airviro (2021). Airviro — Apertum. `https://www.airviro.com/airviro/`. (accessed 2021-05-31T20:29:14Z).

Auvinen, M., Järvi, L., Hellsten, A., Rannik, Ü., and Vesala, T. (2017). Numerical framework for the computation of urban flux footprints employing large-eddy simulation and Lagrangian stochastic modeling. *Geoscientific Model Development*, 10(11):4187–4205.

Brondfield, M., Hutyra, L., Gately, C., Raciti, S., and Peterson, S. (2012). Modeling and validation of on-road CO 2 emissions inventories at the urban regional scale. *Environmental Pollution*, 170:113–123.

Brunekreef, B. and Forsberg, B. (2005). Epidemiological evidence of effects of coarse airborne particles on health. *European Respiratory Journal*, 26(2):309–318.

Burba, G. (2013). *Eddy Covariance Method for Scientific, Industrial, Agricultural, and Regulatory Applications: A Field Book on Measuring Ecosystem Gas Exchange and Areal Emission Rates.* LI-COR Biosciences, Lincoln, Nebraska.

Burba, G. G., McDERMITT, D. K., Grelle, A., Anderson, D. J., and Xu, L. (2008). Addressing the influence of instrument surface heat exchange on the measurements of CO2 flux from open-path gas analyzers. *Global Change Biology*, 14(8):1854–1876.

C40 and ICLEI (2021). Global protocol for community-scale ghg emission inventories, final version. c40 cities climate leadership group and iclei local governments for sustainability. http://www.ghgprotocol.org/city-accounting/. (accessed 2021-06-06T21:59:59Z).

Caiazzo, F., Ashok, A., Waitz, I. A., Yim, S. H. L., and Barrett, S. R. H. (2013). Air pollution and early deaths in the United States. Part I: Quantifying the impact of major sectors in 2005. *Atmospheric Environment*, 79:198–208.

Carslaw, D. C. and Ropkins, K. (2012). Openair — An R package for air quality data analysis. *Environmental Modelling & Software*, 27–28(0):52–61.

Christen, A., Coops, N. C., Crawford, B. R., Kellett, R., Liss, K. N., Olchovski, I., Tooke, T. R., van der Laan, M., and Voogt, J. A. (2011). Validation of modeled carbon-dioxide emissions from an urban neighborhood with direct eddy-covariance measurements. *Atmospheric Environment*, 45(33):6057–6069.

Cloke, J., Boulter, P., Davies, G. P., Hickman, A. J., Layfield, R. E., McCrae, I. S., and Nelson, P. M. (1998). Traffic management and air quality research programme. Technical Report 3011746., Transport Research Foundation Group of Companies.

Conte, M. and Contini, D. (2019). Size-resolved particle emission factors of vehicular traffic derived from urban eddy covariance measurements. *Environmental Pollution*, 251:830–838.

Conte, M., Donateo, A., and Contini, D. (2018). Characterisation of particle size distributions and corresponding size-segregated turbulent fluxes simultaneously with CO2 exchange in an urban area. *Science of The Total Environment*, 622-623:1067–1078.

Crippa, M., Guizzardi, D., Muntean, M., Schaaf, E., Solazzo, E., Monforti-Ferrario, F., Olivier, J., and Vignati, E. (2020a). Fossil CO2 and GHG emissions of all world countries: 2020 report. EUR 30358 EN, Publications Office of the European Union, Luxembourg, 2020, ISBN 978-92-76-21515-8.

Crippa, M., Solazzo, E., Huang, G., Guizzardi, D., Koffi, E., Muntean, M., Schieberle, C., Friedrich, R., and Janssens-Maenhout, G. (2020b). High resolution temporal profiles in the Emissions Database for Global Atmospheric Research. *Scientific Data*, 7(1):121.

Denby, B., Sundvor, I., Johansson, C., Pirjola, L., Ketzel, M., Norman, M., Kupiainen, K., Gustafsson, M., Blomqvist, G., and Omstedt, G. (2013). A coupled road dust and surface moisture model to predict non-exhaust road traffic induced particle emissions (NORTRIP). Part 1: Road dust loading and suspension modelling. *Atmospheric Environment*, 77:283–300.

Environment, U. N. (2017). Cities and climate change. http://www.unenvironment.org/explore-topics/resource-efficiency/what-we-do/cities/cities-and-climate-change. (accessed 2020-11-20T14:55:58Z).

Feigenwinter, C., Vogt, R., and Christen, A. (2012). Eddy Covariance Measurements Over Urban Areas. In Aubinet, M., Vesala, T., and Papale, D., editors, *Eddy Covariance*, pages 377–397. Springer Netherlands, Dordrecht.

Gabusi, V. and Volta, M. (2005). Seasonal modelling assessment of ozone sensitivity to precursors in northern Italy. *Atmospheric Environment*, 39(15 SPEC. ISS.):2795–2804.

Gao, J., Zhou, Y., Wang, J., Wang, T., and Wang, W.-X. (2007). Inter-comparison of WPSTM-TEOMTM-MOUDITM and investigation on particle density. *Huanjing Kexue/Environmental Science*, 28(9):1929–1934.

Gioli, B., Gualtieri, G., Busillo, C., Calastrini, F., Zaldei, A., and Toscano, P. (2015). Improving high resolution emission inventories with local proxies and urban eddy covariance flux measurements. *Atmospheric Environment*, 115:246–256.

Grimmond, C. S. B., King, T. S., Cropley, F. D., Nowak, D. J., and Souch, C. (2002). Local-scale fluxes of carbon dioxide in urban environments: Methodological challenges and results from Chicago. *Environmental Pollution (Barking, Essex: 1987)*, 116 Suppl 1:S243–254.

Gualtieri, G. (2010). Implementing an operational ozone forecasting system based on WRF/CALMET/CALGRID models: A 5-month case study over tuscany, Italy. *Water, Air, and Soil Pollution*, 209(1-4):269–293.

Hadden, D. and Grelle, A. (2017). Net CO2 emissions from a primary boreo-nemoral forest over a 10year period. *Forest Ecology and Management*, 398:164–173.

Hammarström, U. and Karlsson, B. (1994). Fordonskostnader och avgasemissioner för vägplanering (EVA). Technical report, Statens Väg- och Transportforskningsinstitut., VTI notat T 150, Linköping.

HBEFA (2021). HBEFA - Handbook Emission Factors for Road Transport. `https://www.hbefa.net/e/index.html`. (accessed 2021-05-29T15:19:09Z).

Hickman, A. J., Andre, M., Hammarström, U., and Kyriakis, U. (1998). Project Report Se/491/98: Transport Research Laboratory, Emission Standard: Greenhouse Gas. Technical report, Transport Research Laboratory. Registered in England, Number 3011746.TRL Limited.

Hinds, W. C. (1999). *Aerosol Technology: Properties, Behavior, and Measurement of Airborne Particles.* John Wiley & Sons.

Horst, T. W. (1997). A Simple Formula for Attenuation of Eddy Fluxes Measured with First-Order-Response Scalar Sensors. *Boundary-Layer Meteorology*, 82(2):219.

IPCC (2013). IPCC, 2013: Climate Change 2013: The Physical Science Basis. Contribution of Working Group I to the Fifth Assessment Report of the Intergovernmental Panel on Climate Change. [Stocker, T.F., D. Qin, G.-K. Plattner, M. Tignor, S.K. Allen, J. Boschung, A. Nauels, Y. Xia, V. Bex and P.M. Midgley (eds.)]. Cambridge University Press, Cambridge, United Kingdom and New York, NY, USA.

IPCC (2018). Summary for Policymakers. In: Global Warming of 1.5°C. An IPCC Special Report on the impacts of global warming of 1.5°C above pre-industrial levels and related global greenhouse gas emission pathways, in the context of strengthening the global response to the threat of climate change, sustainable development, and efforts to eradicate poverty. [Masson-Delmotte, V., P. Zhai, H.-O. Pörtner, D. Roberts, J. Skea, P.R. Shukla, A. Pirani, W. Moufouma-Okia, C. Péan, R. Pidcock, S. Connors, J.B.R. Matthews, Y. Chen, X. Zhou, M.I. Gomis, E. Lonnoy, T. Maycock, M. Tignor, and T. Water eld (eds.)]. In Press.

Järvi, L., Rannik, Ü., Mammarella, I., Sogachev, A., Aalto, P. P., Keronen, P., Siivola, E., Kulmala, M., and Vesala, T. (2009). Annual particle flux observations over a heterogeneous urban area. *Atmospheric Chemistry and Physics*, 9(20):7847–7856.

Kayhanian, M., McKenzie, E. R., Leatherbarrow, J. E., and Young, T. M. (2012). Characteristics of road sediment fractionated particles captured from paved surfaces, surface run-off and detention basins. *Science of The Total Environment*, 439:172–186.

Kljun, N., Calanca, P., Rotach, M. W., and Schmid, H. P. (2015). A simple two-dimensional parameterisation for Flux Footprint Prediction (FFP). *Geoscientific Model Development*, 8(11):3695–3713.

Lee, J. D., Helfter, C., Purvis, R. M., Beevers, S. D., Carslaw, D. C., Lewis, A. C., Møller, S. J., Tremper, A., Vaughan, A., and Nemitz, E. G. (2015). Measurement of NOx Fluxes from a Tall Tower in Central London, UK and Comparison with Emissions Inventories. *Environmental Science & Technology*, 49(2):1025–1034.

Liu, Z., Hu, B., Ji, D., Wang, Y., Wang, M., and Wang, Y. (2015). Diurnal and seasonal variation of the PM2.5 apparent particle density in Beijing, China. *Atmospheric Environment*, 120:328–338.

Marr, L. C., Moore, T. O., Klapmeyer, M. E., and Killar, M. B. (2013). Comparison of NOx Fluxes Measured by Eddy Covariance to Emission Inventories and Land Use. *Environmental Science & Technology*, 47(4):1800–1808.

Mårtensson, E. M., Nilsson, E. D., Buzorius, G., and Johansson, C. (2006). Eddy covariance measurements and parameterisation of traffic related particle emissions in an urban environment. *Atmos. Chem. Phys.*, page 18.

Matese, A., Gioli, B., Vaccari, F. P., Zaldei, A., and Miglietta, F. (2009). Carbon Dioxide Emissions of the City Center of Firenze, Italy: Measurement, Evaluation, and Source Partitioning. *Journal of Applied Meteorology and Climatology*, 48(9):1940–1947.

McKain, K., Wofsy, S. C., Nehrkorn, T., Eluszkiewicz, J., Ehleringer, J. R., and Stephens, B. B. (2012). Assessment of ground-based atmospheric observations for verification of greenhouse gas emissions from an urban region. *Proceedings of the National Academy of Sciences of the United States of America*, 109(22):8423–8428.

Moore, T. O., Doughty, D. C., and Marr, L. C. (2009). Demonstration of a mobile Flux Laboratory for the Atmospheric Measurement of Emissions (FLAME) to assess emissions inventories. *Journal of Environmental Monitoring*, 11(2):259–268.

Moriwaki, R. and Kanda, M. (2004). Seasonal and Diurnal Fluxes of Radiation, Heat, Water Vapor, and Carbon Dioxide over a Suburban Area. *Journal of Applied Meteorology and Climatology*, 43(11):1700–1710.

Mukherjee, A. and Agrawal, M. (2018). A Global Perspective of Fine Particulate Matter Pollution and Its Health Effects. In de Voogt, P., editor, *Reviews of Environmental Contamination and Toxicology Volume 244*, Reviews of Environmental Contamination and Toxicology, pages 5–51. Springer International Publishing, Cham.

Norman, M. and Johansson, C. (2006). Studies of some measures to reduce road dust emissions from paved roads in Scandinavia. *Atmospheric Environment*, 40(32):6154–6164.

Nosko, O. and Olofsson, U. (2017). Effective density of airborne wear particles from car brake materials. *Journal of Aerosol Science*, 107:94–106.

Qiu, P., Tian, H., Zhu, C., Liu, K., Gao, J., and Zhou, J. (2014). An elaborate high resolution emission inventory of primary air pollutants for the Central Plain Urban Agglomeration of China. *Atmospheric Environment*, 86:93–101.

SLB-analys (2021). Utsläppsdatabaser — SLB-analys. `https://www.slb.nu/slbanalys/utslapp/`. (accessed 2021-06-06T19:55:21Z).

Solazzo, E., Crippa, M., Guizzardi, D., Muntean, M., Choulga, M., and Janssens-Maenhout, G. (2021). Uncertainties in the Emissions Database for Global Atmospheric Research (EDGAR) emission inventory of greenhouse gases. *Atmospheric Chemistry and Physics*, 21(7):5655–5683.

Stagakis, S., Chrysoulakis, N., Spyridakis, N., Feigenwinter, C., and Vogt, R. (2019). Eddy Covariance measurements and source partitioning of CO2 emissions in an urban environment: Application for Heraklion, Greece. *Atmospheric Environment*, 201:278–292.

Stohl, A., Haimberger, L., Scheele, M., and Wernli, H. (2001). An intercomparison of results from three trajectory models. *Meteorological Applications*, 8(2):127–135.

Velasco, E. and Roth, M. (2010). Cities as Net Sources of CO2: Review of Atmospheric CO2 Exchange in Urban Environments Measured by Eddy Covariance Technique. *Geography Compass*, 4(9):1238–1259.

Vogt, M., Nilsson, E. D., Ahlm, L., Mårtensson, E. M., and Johansson, C. (2011a). The relationship between 0.25–2.5 μm aerosol and CO2 emissions over a city. *Atmospheric Chemistry and Physics*, 11(10):4851–4859.

Vogt, M., Nilsson, E. D., Ahlm, L., Mårtensson, E. M., and Johansson, C. (2011b). Seasonal and diurnal cycles of 0.25–2.5 μm aerosol fluxes over urban Stockholm, Sweden. *Tellus. Series B, Chemical and physical meteorology*, 63(5):935–951.

Webb, E. K., Pearman, G. I., and Leuning, R. (1980). Correction of flux measurements for density effects due to heat and water vapour transfer. *Quarterly Journal of the Royal Meteorological Society*, 106(447):85–100.

Zhao, Y., Nielsen, C., Lei, Y., McElroy, M., and Hao, J. (2011). Quantifying the uncertainties of a bottom-up emission inventory of anthropogenic atmospheric pollutants in China. *Atmospheric Chemistry and Physics*, 11(5):2295–2308.